Research Square

Preprints are preliminary reports that have not undergone peer review.
They should not be considered conclusive, used to inform clinical practice,
or referenced by the media as validated information.

Optimizing signal strength in laser communication through extremum-seeking control

Patryk Bartkowiak

patryk.bartkowiak@put.poznan.pl

Poznan Univeristy of Technology

Dariusz Pazderski

Poznan Univeristy of Technology

Article

Keywords:

Posted Date: March 25th, 2026

DOI: https://doi.org/10.21203/rs.3.rs-9127715/v1

License: This work is licensed under a Creative Commons Attribution 4.0 International License.
Read Full License

Additional Declarations: No competing interests reported.

Optimizing signal strength in laser communication through extremum-seeking control*

Patryk Bartkowiak[1,*,+] **and Dariusz Pazderski**[1,+]

[1]Institute of Automatic Control and Robotics, Poznan University of Technology, Poznań, 61-138, Poland
[*]patryk.bartkowiak@put.poznan.pl
[+]these authors contributed equally to this work

ABSTRACT

This paper focuses on extremum-seeking control for a positioning unit, with the aim of maximizing the intensity of the received signal in a laser communication system. It is assumed that the position of the laser beam is not measured explicitly. The essential idea of the proposed feedback mechanism relies on the gradient of the intensity function at the receiver. This gradient is approximated using an averaging method along a spring-like trajectory. The paper presents experimental results obtained with a two-axis astronomical mount and a set of laser communication devices. These results effectively demonstrate the efficacy of the proposed control algorithm and confirm the high accuracy of the positioning communication units in real-time scenarios.

1 Introduction

Laser communication systems play an important role in a spectrum of tasks, due to their unique properties and versatility[1–4]. In telecommunications, they are at the forefront of high-speed data transmission, offering greater bandwidth and lower latency compared to traditional radio frequency systems[5,6]. Laser technology facilitates the transfer of large volumes of data, including images, videos, and scientific measurements, with greater efficiency and reliability. Laser communication systems are valuable in space missions, where high-bandwidth communication is necessary between spacecraft, satellites, and ground stations[7,8]. They are utilized in military applications for secure and jam-resistant communication channels, where it is necessary for real-time data exchange[9]. In certain applications, it is essential to accurately position both the transmitting and receiving devices to ensure that the laser beam precisely aligns with the center of the detection device sensor. Effective searching for the signal, its recovery, and also maintaining a high signal-to-noise ratio is crucial to ensuring reliable transmission including continuity and error-free data transfer. This requires robust positioning and tracking algorithms to increase beam alignment efficiency and enhance signal reception. Therefore, much research is being carried out on methods for positioning the laser beam in the most effective way. Typically, this task is accomplished using cameras or four-quadrant detectors[10]. However, challenges arise when only the intensity of the received beam is accessible.

This limitation motivates the search for advanced control strategies that can exploit intensity feedback alone to optimize signal reception. In this context, extremum-seeking control (ESC) provides a powerful model-free optimization framework. ESC algorithms operate in real time and do not require explicit knowledge of the system dynamics. Instead, they iteratively adjust the control inputs to drive the system toward the extremum of an unknown performance map, such as the maximum of the received optical power[11–15]. However, ESC has some drawbacks, the most notable being its relatively slow convergence to the optimum compared with model-based adaptive controllers[16]. This limitation arises from the need to inject perturbations and rely on averaged gradient estimates, which inherently slows down the adaptation process[17]. Nevertheless, in laser communication systems, the underlying intensity map can vary significantly under changing environmental conditions, such as humidity or turbulence, which makes performance model–based approaches less reliable. A well-known challenge in extremum seeking is the presence of local extrema, which can mislead the controller and prevent convergence to the true global optimum. As discussed in[18], global convergence is not always guaranteed in such cases, and the algorithm may stall at a suboptimal point, depending on the excitation amplitude and tuning strategy. Another important challenge in extremum seeking control arises from delays in the input and output channels. Such delays are common in practical systems and can significantly degrade performance or even destabilize the closed-loop scheme. Recent advances, such as the predictor-based approach proposed in[19], address nonconstant and state-dependent delays by combining perturbation-based gradient estimation with backstepping and averaging theory.

This paper addresses the challenge of extremum-seeking control in the context of positioning a transmitting device to maximize the signal received by a receiver detector. In the specific control problem investigated here, the gradient of the

intensity function remains unknown. To overcome this limitation, we employ a gradient-based technique and an averaging approach for its reconstruction . The proposed algorithm is defined in the continuous time domain and leverages a periodic spring-like trajectory, enabling gradient approximation within the vicinity of a point in the configuration space of the positioning mechanical system. Furthermore, a radius adaptation law is introduced to mitigate the influence of local extrema and guide the system toward the global extremum of the intensity map.

In the literature, extremum-seeking methods are typically developed for one-dimensional setups, and their extension to higher dimensions often leads to increased design and tuning complexity. In contrast, our approach is specifically tailored for two-dimensional problems, making it simpler to tune and implement.

The main contribution of this paper lies in the formal description of the feedback-based algorithm and its practical implementation under laboratory conditions. To demonstrate functionality and conduct experimental research, a dedicated research platform has been established. This platform utilizes a custom-designed astronomical mount system developed and built at the Institute of Automatic Control and Robotics of the Poznan University of Technology[20,21].

Throughout this paper, the notation $\|x\|$ denotes the Euclidean norm (i.e. ℓ_2); $|x|$ denotes ℓ_∞ norm.

2 Control problem

Let us consider a scenario where a receiver detects a spot from a laser beam, as depicted in Fig. 1. The intensity of the beam, described by a non-negative function $\mu \geq 0$, varies depending on the beam spot position relative to the detector. That is, the peak intensity is obtained when the beam center perfectly aligns with the detector center. Achieving such a configuration of the transmission system constitutes the main control objective investigated in this paper. It is assumed that the orientation of

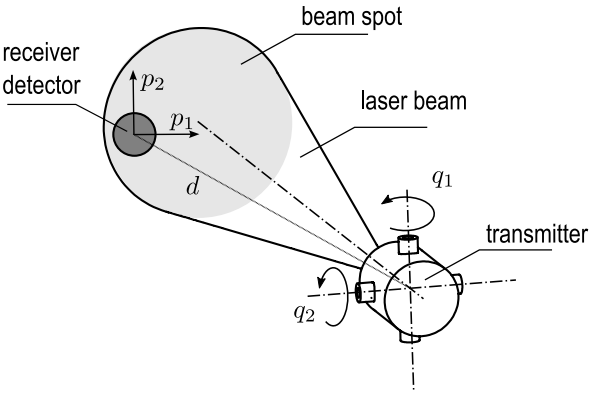


Figure 1. The intensity of the laser beam seen by the detector.

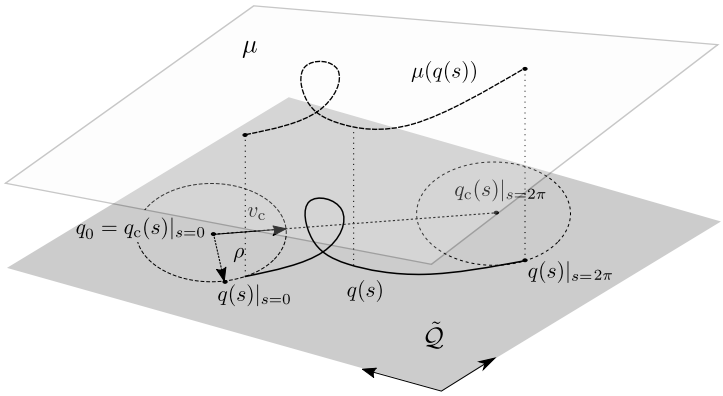


Figure 2. The principle of the gradient determination method considered in the paper.

the transmitter unit can be changed in two axes, hence its configuration can be described as: $q = [q_1\ q_2]^{\mathrm{T}} \in \mathcal{Q} = S^1 \times S^1$. Its kinematic model satisfies

$$\dot{q} = v_q, \tag{1}$$

where $v \in \mathbb{R}^2$ constitutes control input. Then the following extremum-seeking control problem can be stated.

Problem 1. *Find a control law $v_q = v_q(\cdot)$ that allows maximizing the intensity μ assuming that μ and configuration q are measurable variables. More precisely, we expect that the control algorithm will ensure that the following limit relationships hold*

$$\lim_{t\to\infty} \mu(t) = \mu_m, \ \lim_{t\to\infty} q(t) = q_m, \tag{2}$$

where $q_m \in \mathcal{Q}$ denotes the configuration for which the intensity reaches maximum value μ_m.

3 Control algorithm

From the perspective of solving the control problem, it is essential to distinguish between two cases, considering the available information. For this purpose, let us introduce the set Ω in $\mathcal{Q}$ for which the reception of a laser beam by the receiver is ensured, i.e. $\Omega = \{q \in \mathcal{Q} :\ \mu \geq \bar{\mu}\}$, where $\bar{\mu} > 0$ is a certain threshold. When $q \in \mathcal{Q} \setminus \Omega$ the laser beam falls outside the detection area

of the receiver, leading to the intensity μ that is nearly zero. The control objective in this case is to reach a configuration $q \in \Omega$ that enables the detection of the beam. In the second scenario, the laser beam illuminates the receiver sensor, and the signal intensity surpasses a certain threshold, $\bar{\mu}$. In this situation, a feedback controller can be designed to seek the maximum intensity. Both scenarios are considered in this Section.

3.1 Coverage open-loop control

Taking into account the topology of the configuration space arising from rotations around independent axes, a circular-based motion pattern can be chosen. More precisely, assuming that $q \in \mathscr{Q} \setminus \Omega$ we propose to apply a simple strategy to cover the configuration space using the following spiral trajectory

$$q_{\mathrm{o}}(t) = rt \begin{bmatrix} \cos(\omega t) \\ \sin(\omega t) \end{bmatrix} + q_{\mathrm{o}}(0), \tag{3}$$

where $q_{\mathrm{o}}(0) \in \mathscr{Q}$ is an offset, $\omega \in \mathbb{R} \setminus \{0\}$ and $r \in \mathbb{R}_+$ are parameters. The input v in (1) can be easily determined by taking the time derivative of (3). The coverage stage lasts as long as the intensity $\mu \leq \bar{\mu}$, that is $q \in \mathscr{Q} \setminus \Omega$.

3.2 Preliminary feedback control

Initially, we assume that μ has no local minima and the only critical point is the maximum. Thus, it is possible to search for the maximum based on the gradient $\nabla_q \mu = \frac{\partial \mu}{\partial q}$. This gradient enables determining a vector field, which locally describes the velocity at any point $q \in \mathscr{Q}$. Thus, the following feedback can be considered

$$v_q = k_q \nabla_q^{\mathrm{T}} \mu, \tag{4}$$

with $k_q > 0$ being a gain, which ensures that control objectives (2) are satisfied.

However, formula (4) cannot be used directly because the gradient's explicit form is unknown. Therefore, it is crucial to find a method for estimating the gradient during control.

3.3 Gradient estimation

It is assumed that the only available information is the value of the function μ at the point q, and based on these data the gradient $\nabla_q \mu$ should be restored. For the introduction of the method for computing the gradient, we first consider the case of a uniformly distributed function that has a single global extremum, under the assumption that μ is quadratic. Consider the set $\tilde{\mathscr{Q}} \subset \mathbb{R}^2$ and define the intensity function $\mu : \tilde{\mathscr{Q}} \to \mathbb{R}$ that satisfies $\forall q \in \tilde{\mathscr{Q}},\ \mu = -\frac{1}{2} q^{\mathrm{T}} P q + \mu_{\mathrm{m}}$, where $P \in \mathbb{R}^{2\times 2}$ is the positive definite symmetric matrix. Assume that the gradient is considered on a curve that originates at $q_0 \in \tilde{\mathscr{Q}}$, that is: $q_{\mathrm{c}}(s) = q_0 + \int_0^s v_{\mathrm{c}}(\tau)\,\mathrm{d}\tau$, while $v_{\mathrm{c}}(s) \in \mathbb{R}^2$ is a tangent vector, and $s \in \mathscr{I} \subset \mathbb{R}_{\geq 0}$ is the parameterization variable. In the neighborhood of $q_{\mathrm{c}}(s)$, we further introduce the following cycloid

$$q_{\mathrm{s}}(s) = q_{\mathrm{c}}(s) + \rho(s) w(s) \in \tilde{\mathscr{Q}}, \tag{5}$$

where $\rho(s) = \int_0^s v_\rho(\tau)\,\mathrm{d}\tau + \rho_0 \in [\underline{\rho}, \bar{\rho}]$ denotes a positive radius with an initial value $\rho_0 > 0$, while $v_\rho(s) \in \mathbb{R}$ represents the rate at which the radius changes, and $w(s) = \begin{bmatrix} \cos(s) & \sin(s) \end{bmatrix}^{\mathrm{T}}$ defines the excitation function.

Proposition 1. *The following expression*

$$\widetilde{\nabla}_q \mu = (\pi \rho_0)^{-1} \int_0^{2\pi} \mu'(s)\, \xi^T(s) \mathrm{d}s, \tag{6}$$

where $\mu'(s) = \frac{\partial \mu}{\partial s}$ and $\xi(s) = w'(s)$ defines an approximation of the gradient $\nabla_q \mu$ computed at point $q_0 \in \tilde{Q}$, whose approximation error satisfies

$$\|\widetilde{\nabla}_q \mu - \nabla_q \mu\| \leq c_v \|v_c\| + c_\rho |v_\rho| \tag{7}$$

for some positive constants c_v and c_ρ, provided that $\|v_c\|$ and $|v_\rho|$ are sufficiently small.

Proof. Computing $\mu'(s) = \frac{\partial \mu}{\partial s} = \frac{\partial \mu}{\partial q} \frac{\partial q}{\partial s}\big|_{q=q_{\mathrm{s}}}$ and using (5) one concludes that

$$q_{\mathrm{s}}'(s) = v_{\mathrm{c}}(s) + v_\rho(s) w(s) + \rho_0 \xi(s). \tag{8}$$

Recalling the assumed form of μ it is clear that $\nabla_q \mu = \frac{\partial \mu}{\partial q} = -q^{\mathrm{T}} P$. As a result, (6) can be written as

$$\widetilde{\nabla}_q \mu = -(\pi \rho_0)^{-1} \chi(s) P, \tag{9}$$

where $\chi(s) = \int_0^{2\pi} q_s^{\mathrm{T}}(s) q_s'(s) \xi^{\mathrm{T}}(s) \mathrm{d}s$. Evaluating the integral in (9), one obtains: $\chi(s) = \rho_0 \pi q_0{}^{\mathrm{T}} + R_v(v_c, v_\rho)$, where $\|R_v(v_c, v_\rho)\| = \mathscr{O}(\|v_c\| + |v_\rho|)$ collects the remaining contributions that depend on v_c and v_ρ. Hence, in the regime $\|v_c\| \to 0$ and $|v_\rho| \to 0$ the integral is dominated by the leading-order term, so that $\chi(s) \sim \rho_0 \pi q_0{}^{\mathrm{T}}$. Thus, neglecting these terms as they are of lower significance, one can show that

$$\widetilde{\nabla}_q \mu \approx -(\pi \rho_0)^{-1} \rho_0 \pi q_0{}^{\mathrm{T}} P = -q_0{}^{\mathrm{T}} P. \tag{10}$$

□

Remark 1. *The method can be interpreted geometrically as shown in Fig. 2. The path (5) can conveniently be represented as a composition of circular curve with radius ρ and a linear displacement of the circle center, whose coordinates are given by q_c, in the direction determined by vector v_c. In the frame fixed at the circle center, the gradient $\widetilde{\nabla}_q \mu$ is restored within one full rotation along the circle.*

3.4 Local extrema problem

The laser beam intensity distribution often exhibits multiple local extrema, due to diffraction and interference phenomena, which may cause the gradient-based control algorithm to converge to undesired stationary points. It is essential to analyze the properties of the gradient estimation near these extrema to better understand the conditions under which the control law may become trapped. This analysis provides the foundation for the design of the adaptation mechanism, which aims to ensure that the control system can overcome local extrema and maintain progress toward the global optimum.

Let the intensity μ have one isolated local maximum $\mu_{\mathrm{l}} = \mu(q_{\mathrm{l}})$ and the global maximum $\mu_{\mathrm{m}} = \mu(q_{\mathrm{m}})$. Denote by $d_{\mathrm{m}} = q_{\mathrm{m}} - q$ a vector which indicates a feasible transition from q to the global maximum. To quantify the alignment of the gradient approximation with the global ascent, we introduce the quality indicator $J_m(\widetilde{\nabla}_q \mu) = \cos\beta = \frac{\widetilde{\nabla}_q \mu \, d_{\mathrm{m}}}{\|\widetilde{\nabla}_q \mu\| \|d_{\mathrm{m}}\|}$, where β denotes the angle between two vectors. Using this indicator, one can state that if, over the interval $\forall s \in [0,1]$, $q_{\mathrm{c}} = s q_{\mathrm{l}} + (1-s) q_{\mathrm{m}}$, with $J_m(\widetilde{\nabla}_q \mu\big|_{q=q_{\mathrm{c}}}) > 0$, then $q_{\mathrm{c}}(s)$, evolving in the direction specified by $\widetilde{\nabla}_q \mu$, can reach the global maximum, overcoming a local maximum at which the true gradient $\nabla_q \mu = 0$. To introduce a mechanism that facilitates convergence toward the global extremum, it is necessary to reduce the sensitivity of $\widetilde{\nabla}_q \mu$ to local extrema – that is, to make $\widetilde{\nabla}_q \mu$ less precise with respect to the local gradient $\nabla_q \mu$. This can be achieved by appropriately tuning the radius ρ, which is a key parameter in $\widetilde{\nabla}_q \mu$. We now consider the following conjecture.

Conjecture 1. *There exists such a radius ρ that $J_m(\widetilde{\nabla}_q \mu) > 0$ for $s \in [0,1]$, $q_c = s q_l + (1-s) q_m$.*

Calculating $\widetilde{\nabla}_q \mu$ using (6) and neglecting constant scaling terms, we consider the following integral:

$$I(\rho) = \int_0^{2\pi} \frac{\partial \mu}{\partial q}\Big|_{q=q_{\mathrm{s}}} \xi(s) \, \xi(s)^{\mathrm{T}} \, \mathrm{d}s, \tag{11}$$

which can be used in the indicator $J_m(I)$ instead of $\widetilde{\nabla}_q \mu$. Assuming that μ is sufficiently smooth near q_{c} so that the Taylor series of $\frac{\partial \mu}{\partial q}\big|_{q=q_{\mathrm{s}}}$ in the vicinity of q_{c} converges, and recalling (5), the i-th component ($i = 1, 2$) of the gradient $\frac{\partial \mu}{\partial q_i}\big|_{q=q_{\mathrm{s}}}$ can be expanded as follows:

$$\frac{\partial \mu}{\partial q_i}\Big|_{q=q_{\mathrm{s}}} = \sum_{n=0}^{\infty} \frac{\rho^n}{n!} (D_w)^n \frac{\partial \mu}{\partial q}\Big|_{q=q_{\mathrm{c}}}, \tag{12}$$

where $n \in \mathbb{Z}_{\geq 0}$ and $D_w := \cos s \, \frac{\partial}{\partial q_1} + \sin s \, \frac{\partial}{\partial q_2}$ denotes the differential operator corresponding to the directional derivative along the circle at angle s. Additionally, using a binomial expression, we can find that: $(D_w)^n = \sum_{j=0}^{n} \binom{n}{j} \cos^{n-j} s \, \sin^j s \, \partial_{q_1}^{n-j} \partial_{q_2}^{j}$. Substituting this into (12) and then into (11) and integrating termwise, we obtain

$$I_i(\rho) = \sum_{n=0}^{\infty} \frac{\rho^n}{(n)!} \sum_{j=0}^{n} \binom{n}{j} J_{j,\, n-j+1} \, D_{n,j,i}, \tag{13}$$

where $J_{n,j} := \int_0^{2\pi} \sin^n s \cos^j s \, ds$ and $D_{n,j,i} := \partial_{q_1}^{n-j} \partial_{q_2}^{j} \partial_{q_i} \mu|_{q=q_c}$. We can notice that for odd n and j, the integrand $\sin^n s \cos^j s$ has a vanishing mean over a full period. Thus, only even values $n = 2k$ and $j = 2m$ contribute, so the integral (13) can be rewritten in the following form

$$I_i(\rho) = \sum_{k=0}^{\infty} \frac{\rho^{2k}}{(2k)!} \sum_{m=0}^{k} \binom{2k}{2m} J_{2m,\,2(k-m)+2} \, D_{2k,2m,i}. \tag{14}$$

Remark 2. *To investigate the existence of ρ such that $J_m(I) > 0$, one can analyze the finite expansion (14). We can state the following:*

1. *If $J_m(D_{0,0}) > 0$, then sufficiently small ρ ensures that $J_m > 0$. This corresponds to the case when the true gradient is sufficient to determine a proper direction.*
2. *If $J_m(D_{0,0}) < 0$, it is still possible to obtain $J_m > 0$ by using larger values of ρ, due to the contribution of higher-order terms. Whether this occurs depends on the signs and magnitudes of $D_{2k,2m,i}$ for $k \geq 1$.*

To further investigate this issue, we select a specific model of μ. Let us assume that μ is a polynomial of degree 4, which is the lowest order that allows for the existence of both local and global extrema. Then $\partial_{q_i}\mu$ is cubic, so all partial derivatives of order higher than 3 vanish. Since angular integrals eliminate odd powers, only the terms with $n = 0$ and $n = 2$ contribute to I_i. Integrals then become

$$I_i(\rho) = \pi D_{0,0,i} + \frac{\pi\rho^2}{8} (D_{2,0,i} + D_{2,2,i}) \tag{15}$$

and at this stage, we can verify both indicators $J_m(D_{0,0})$ and $J_m(D_2)$, where $D_2 = D_{2,0} + D_{2,2}$, as shown in Fig. 3. Analyzing both figures, we can see that by establishing an appropriately large radius $\rho \geq \rho^\star$, the magnitude of D_2 dominates, making it possible to overcome local extrema. This property provides a key motivation for introducing a tuning mechanism that dynamically adjusts this radius, as discussed in the next section.

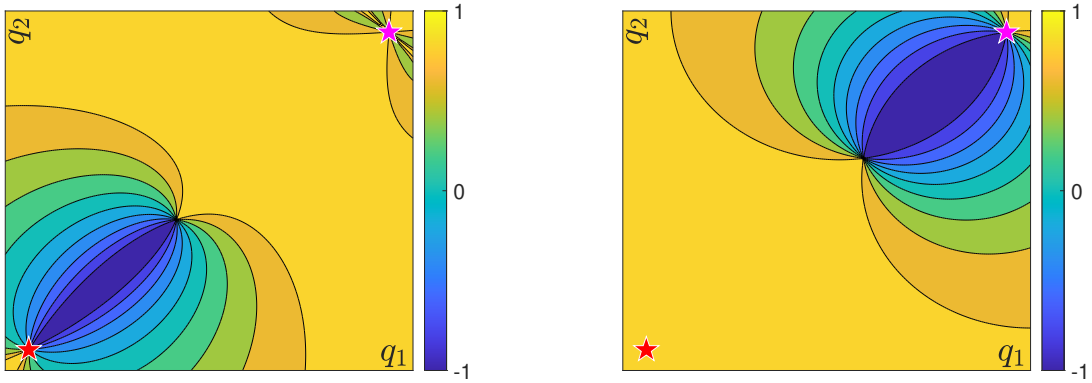


Figure 3. Indicators illustrated for an example fourth-degree polynomial μ: (a) $J_m(D_{0,0})$; (b) $J_m(D_2)$. The red star marks the local maximum, while the purple star marks the global maximum.

3.5 Radius tuning

Based on the analysis of the local maximum problem, the radius ρ can be tuned to increase when a local extremum is encountered and decrease when a global extremum is reached. A local extremum occurs when the local gradient $\nabla_q \mu \to 0$ while the intensity value μ remains below the maximum intensity μ_m, whereas a global extremum is identified when $\nabla_q \mu \to 0$ and $\mu \to \mu_\mathrm{m}$.

As the exact value of $\mu_\mathrm{c} = \mu(q_\mathrm{c})$ cannot be directly measured, we exploit the average intensity around the circle $\bar{\mu}_c = \frac{1}{2\pi} \int_0^{2\pi} \mu(q_\mathrm{s}(s)) ds$, where the approximation error satisfies $|\mu_\mathrm{c} - \bar{\mu}_c| \leq \varepsilon$.

We propose to modulate the radius ρ using the following preliminary adaptation law: $\rho' = f_\rho(\cdot)$, where f_ρ is defined below.

Definition 1. *Let the mapping function $f_\rho(\cdot)$ be a convex combination:*

$$f_\rho = w f_\mu(\bar{\mu}_c) + (1-w) f_\nabla(|\widetilde{\nabla}_q \mu|) \tag{16}$$

with $w \in [0,1]$ determining the relative contribution of each component. The first component, f_μ, captures the dependence on the average intensity around the circle and can be defined as

$$f_\mu = (\mu_m - \bar{\mu}_c)^{-\mu_p}(c_2\bar{\mu}_c^2 + c_1\bar{\mu}_c + c_0), \tag{17}$$

where the coefficients are given by $c_0 = \bar{v}_\rho \mu_m^{\mu_p}$, $c_1 = -\bar{v}_\rho \mu_p \mu_m^{(\mu_p-1)}$, $c_2 = \bar{v}_\rho \mu_t^{-2}\left(\mu_p \mu_m^{(\mu_p-1)}\mu_t - \mu_m^{\mu_p}\right)$. The second component, f_∇, describes the dependence on the gradient of the intensity distribution and can be formulated as follows

$$f_\nabla = \begin{cases} b_3|\widetilde{\nabla}_q\mu|^3 + b_2|\widetilde{\nabla}_q\mu|^2 + b_0, & |\widetilde{\nabla}_q\mu| \in [0,\rho_t], \\ \rho_k\left(1 - \left(\frac{\rho_t}{|\widetilde{\nabla}_q\mu|}\right)^{\rho_p}\right)^2, & |\widetilde{\nabla}_q\mu| \in (\rho_t,\infty), \end{cases} \tag{18}$$

where $b_0 = \bar{v}_\rho$, $b_2 = -\frac{3\bar{v}_\rho}{\rho_t^2}$, $b_3 = \frac{2\bar{v}_\rho}{\rho_t^3}$.

Remark 3. *Consider the case where $w = 1$, that is, the adaptation law depends solely on the function f_μ. By setting the design parameter μ_t such that $\mu_t > \mu_l + \varepsilon$, it is guaranteed that $v_\rho > 0$ whenever the average intensity $\bar{\mu}$ falls below the threshold μ_t. Consequently, since the adaptation law continues to increase the radius ρ whenever $\bar{\mu} < \mu_t$, the radius eventually reaches a critical value $\rho^\star$, enabling convergence to the global extremum.*

3.6 Feedback design

Returning to the problem of state feedback design based on the preliminary formula (4), we make the parameterizing variable s time-dependent by redefining $s = \nu t$, where ν is the oscillation frequency. Hence, computing velocity $\dot{q}_\mathrm{s}$ based on (8), we have: $\dot{q}_\mathrm{s} = \nu\left(v_\mathrm{c}(t) + v_\rho(t)w(\nu t) + \rho_0\xi(\nu t)\right)$. Consequently, the gradient is estimated continuously at the point $q_\mathrm{c}(t-\tau)$ over the moving horizon $[t-\tau, t]$, where $\tau = \frac{2\pi}{\nu}$. Hence, the expression (6) is redefined as follows

$$\widetilde{\nabla}_q\mu(t) = \left(\pi\rho\left(t - \tfrac{2\pi}{\nu}\right)\right)^{-1}\int_{\nu t - 2\pi}^{\nu t} \mu'(s)\,\xi^\mathrm{T}(s)\mathrm{d}s. \tag{19}$$

Now, recalling feedback (4), we can state the following.

Proposition 2. *The control law*

$$v_q(t) = \nu\left(v_c(t) + v_\rho(t)w(\nu t) + \rho_0\xi(\nu t)\right), \tag{20}$$

$$v_c(t) = k_q\widetilde{\nabla}_q^T\mu(t), \tag{21}$$

$$v_\rho(t) = k_\rho f_\rho(\bar{\mu}_c(t), |\widetilde{\nabla}_q\mu(t)|) \tag{22}$$

with gain $k_q > 0$ and $k_\rho > 0$ chosen small enough and $\nu > 0$ large enough, ensures that for $q(0) \in \Omega$, $\lim_{t\to\infty} q_c(t) = q_l$.

Proof. Consider the following Lyapunov function candidate: $V = \frac{1}{2}\tilde{\mu}^2$, where $\tilde{\mu} = \mu_\mathrm{m} - \mu \geq 0$ denotes the intensity error defined with respect to the maximum intensity value. Taking the time derivative of V and employing (21), we obtain: $\dot{V} = -k_q\tilde{\mu}\nabla_q\mu\,\widetilde{\nabla}_q^\mathrm{T}\mu$. Comparing the gradient $\nabla_q\mu$ with its approximation, we can write: $\widetilde{\nabla}_q\mu = \nabla_q\mu + R_\nabla$, where R_∇ denotes the approximation error. Thus, the derivative $\dot{V}$ becomes

$$\dot{V} = -k_q\tilde{\mu}\left(\|\nabla_q\mu\|^2 + \nabla_q\mu R_\nabla^\mathrm{T}\right) \leq -k_q\tilde{\mu}\left(\|\nabla_q\mu\|^2 - \|\nabla_q\mu\|\|R_\nabla\|\right). \tag{23}$$

From the assumption that the real gradient satisfies the Lipschitz condition (at least in the vicinity of the local maximum q_l), we can write: $\|\nabla_q\mu(t) - \nabla_q\mu(t-\tau)\| \leq c_q\|q_\mathrm{c}(t) - q_\mathrm{c}(t-\tau)\|$. Within the time interval τ, one can bound the change of q_c as: $\|q_\mathrm{c}(t) - q_\mathrm{c}(t-\tau)\| \leq \tau\sup_{\zeta\in[t-\tau,t]}\|v_\mathrm{c}(\zeta)\| \lesssim c_v\tau\|v_\mathrm{c}(t)\|$, where $c_v > 0$ is a bounded positive constant provided that $\|\dot{v}_c\|/\|v_\mathrm{c}\|$ is bounded. As a result, one can state the following: $\|\nabla_q\mu(t-\tau)\| \leq \|\nabla_q(t)\| + c_\tau\tau\|v_\mathrm{c}(t)\|$. Since $\widetilde{\nabla}_q\mu = \nabla_q\mu(t-\tau) + R_v$, where R_v is the residual due to the terms v_c and v_ρ, one has: $\|\widetilde{\nabla}_q\mu(t)\| \leq \|\nabla_q\mu(t-\tau)\| + \|R_v\| \leq \|\nabla_q\mu(t)\| + \bar{c}_v\|v_\mathrm{c}(t)\| + c_\rho|v_\rho(t)|$, where $\bar{c}_v = c_v + c_\tau\tau$. Recalling (21) one obtains

$$\|\widetilde{\nabla}_q\mu\| \leq \tfrac{1}{1-\bar{c}_v k_q}\|\nabla_q\mu\| + \tfrac{1}{1-\bar{c}_v k_q}c_\rho|v_\rho|. \tag{24}$$

Hence, $\|R_\nabla\| \leq \frac{\bar{c}_v k_q}{1-\bar{c}_v k_q}\|\nabla_q\mu\| + \frac{1}{1-\bar{c}_v k_q}c_\rho|v_\rho|$ and $\dot{V} \leq -k_q\tilde{\mu}\left(\frac{1-2\bar{c}_v k_q}{1-\bar{c}_v k_q}\|\nabla_q\mu\|^2 - \frac{c_\rho}{1-\bar{c}_v k_q}|v_\rho|\|\nabla_q\mu\|\right)$. Therefore, for $k_q \in (0, \frac{1}{2\bar{c}_v})$, the derivative $\dot{V}$ is negative for $\|\nabla_q\mu\| > \frac{c_\rho}{1-2\bar{c}_v k_q}$. In addition, assuming that v_ρ approaches zero, $\dot{V}$ becomes negative definite. This indicates that the $q_\mathrm{c}(t)$ converges to the local maximum q_l at which $\nabla_q\mu = 0$. □

Remark 4. *The presented proof deals with the convergence of the trajectory q_c to the local maximum. However, the globalization of this result is possible due to the adaptation law (22). Namely, by cautiously tuning ρ using low gain k_ρ, the closed-loop system cannot get stuck at the local maxima, provided that μ is less than the assumed threshold. This is ensured by the properties of the mapping function f_ρ in (16). Therefore, increasing the parameter ρ present in $\widetilde{\nabla}_q \mu$ allows for the attenuation of the effects of local extrema and the recovery of the direction required to reach the global maximum.*

Remark 5. *The stability of the closed-loop control system is maintained when control gains are selected to be small enough. In addition, to quantify the real limitations of the controlled mechanical system, its joint velocities, $v_q = \dot{q}$, should stay within a feasible range. To ensure this, one can redefine v_c by using the following scaling procedure:*

$$\tilde{v}_c = \max\left\{1, \|\bar{v}^{-1} v_c\|_\infty\right\}^{-1} v_c, \tag{25}$$

where $\bar{v}_c > 0$ stands for the assumed maximum absolute value of each component of v_c. Similarly, the control signal v_ρ can be saturated to ensure that its magnitude does not exceed the prescribed bound $\bar{v}_\rho$ according to the following formula

$$\tilde{v}_\rho = \max\left\{-\bar{v}_\rho,\ \min\{v_\rho,\ \bar{v}_\rho\}\right\}. \tag{26}$$

4 Experiment

4.1 Setup

In the experimental study, we have employed the AstroLight laser communication kit, which facilitates one-way transmission with a throughput of 10 Mbps using an infrared laser operating at a wavelength of 1.5 µm. The receiver has been mounted on a tripod, while the transmitter has been affixed to the altitude axis of an astronomical horizontal mount, see Figs. 4a and 4b. The



(a) (b)

Figure 4. Experimental setup: (a) the transmitter and the receiver from the AstroLight laser communication kit; (b) the astronomical mount operating in Skylab observatory developed at the Institute of Automatic Control and Robotics, Poznan University of Technology.

transmitter at the observatory and the receiver at the laboratory in the institute building were placed at a distance of $d = 100$ m from each other. Here, it is worth interpreting the trajectory within the task space, particularly in proximity to the receiver. The relationship between points $q = [q_1, q_2]^{\mathrm{T}}$ and $p = [p_1, p_2]^{\mathrm{T}}$, defined in the configuration and task space, respectively, is depicted in Fig. 1. Assuming that angle deviations are small, one can easily conclude that a circular trajectory with radius ρ can be approximated to the circular trajectory with radius $a \approx \rho d$.

The algorithm described in Section 3 has been implemented indirectly, taking advantage of the cascade-like structure of the control system designed specifically for the mount. To be more precise, instead of controlling the mount at the velocity level, the reference trajectory q_{ref} is computed based on formulas (3) and (20)-(21). The tracking of the reference trajectory with high precision is guaranteed by the low-level motion controller, taking advantage of the ADRC structure[22].

The high-level controller logic was implemented as a standalone Linux desktop application in C++, using the FTDI and ADS1115 libraries, along with the ASTCom communication library. Leveraging ASTCom, the application facilitates seamless

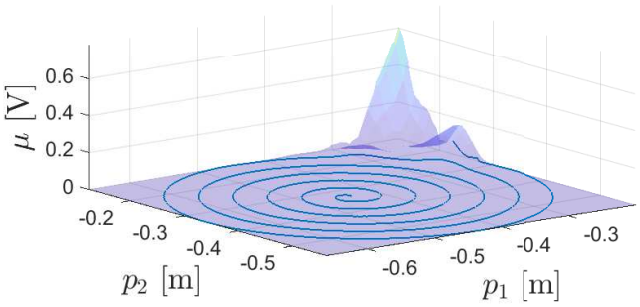


Figure 5. The spiral trajectory recorded in the covering phase of the algorithm for $r = 2\text{e-}5$ rad/s and $\omega = 0.31$ rad/s.

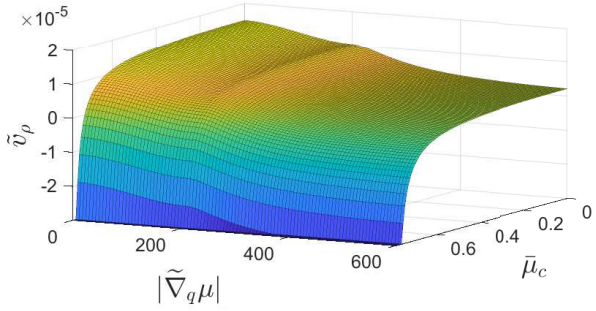


Figure 6. Control signal $\tilde{v}_\rho$ as a function of the average intensity $\bar{\mu}_c$ and the ℓ_∞ norm of the gradient $|\widetilde{\nabla}_q \mu|$ for set parameters.

communication with the telescope system, enabling tasks such as querying available variables, modifying parameters, and executing functions to control the mount. The feedback loop operated at a stable frequency of 20 Hz.

The laser beam intensity μ was measured from the analog voltage provided by the detector using an ADS1115 module featuring a 16-bit ADC operating at up to 860 sps. Differential measurement mode was applied, and the ADS1115 was connected to an FT232H interface on a custom-designed electrical board, enabling direct voltage measurements from the receiver. The FT232H is a USB-to-multi-protocol interface chip that allows a computer to communicate directly with external modules and sensors. In this setup, communication between the ADS1115 and FT232H was established via the I^2C protocol, while the connection between the PC (running the C++ application) and the FT232H used the UART protocol.

4.2 Results

In the preliminary experiment, the dispersion pattern of the laser signal is identified using the spiral trajectory (3). The intensity function μ obtained in the task space is illustrated in Fig. 7. It can be noticed that for the considered communication system, the receiver output voltage becomes saturated, which is manifested by a flattening of the obtained function in the range of the maximum intensity of the laser beam. The laser beam intensity does not exhibit a uniform distribution, and local extrema can be observed in the plot.

The trajectory (3) has also been employed in the covering phase of the positioning algorithm, although with different parameter values. Example results of this phase are presented in Fig. 5, while the trajectory is shown in the task space.

To further facilitate the interpretation of the obtained data, we add an offset to the original configuration q to guarantee that for $q_\text{m} = [0\ 0]^\text{T}$ the maximum intensity $\mu = \mu_\text{m}$ is reached. The covering phase is completed when the measured voltage signal exceeds a given threshold value $\bar{\mu}$, that is, q reaches Ω; then the next phase of the algorithm is triggered. For all the experiments presented, the $\bar{\mu}$ threshold remained constant at 0.1 V.

In the following experimental cases, the feedback control performance is taken into account. In all experiments presented, the following parameters have been set as: $\mu_\text{m} = 0.78$ V, $\bar{v}_\rho = 3\text{e-}5$ rad/s (3 mm/s), $\rho_0 = 1\text{e-}3$ rad (10 cm), $\bar{\rho} = 1\text{e-}3$ rad, $k_\rho = 0.5$, $\mu_t = 0.7$ V, $\mu_p = 0.9$, $\rho_t = 200$, $\rho_p = 3$, $\rho_k = 6\text{e-}5$ rad/s, $w = 0.7$. The dependence of the control signal $\tilde{v}_\rho$ on the average intensity $\bar{\mu}_c$ and the ℓ_∞ norm of the gradient approximation $|\widetilde{\nabla}_q \mu|$ is illustrated in Fig. 6. The surface illustrates the combined influence of both variables on the adaptive radius adjustment for set parameters. In Figs. 8 and 9 results obtained for gradient-based control are shown. For this case, the subsequent parameters were specified as: $\nu = 0.1$ Hz, $k_q = 2\text{e-}7$, $\bar{v}_\text{c} = 1\text{e-}5$ rad/s (1 mm), $\underline{\rho} = 2\text{e-}4$ rad (2 cm). The first drawing presents a three-dimensional graph that depicts the path $q \in \mathscr{Q}$ overlaid on a surface plot illustrating the laser beam intensity distribution. The second figure shows time plots of the configuration q, control signals $\tilde{v}_c$, radius ρ, control signal v_ρ and the intensity μ. Due to the saturation of the signal μ near the top of the laser beam distribution, the gradient value decreases, resulting in small values of the control signal. In Figure 10a, the system response is illustrated for three different initial values of configuration q, confirming the robustness of the control algorithm across varying initial states. For this experimental case, the minimum radius was changed to $\underline{\rho} = 5\text{e-}5$ rad (5 mm). The influence of the frequency ν on the algorithm operation has also been examined. For this purpose, the results for $k_q = 2\text{e-}7$, $\bar{v}_\text{c} = 1\text{e-}5$ rad/s, $\underline{\rho} = 5\text{e-}5$ rad (5 mm) and the increased value of $\nu = 0.2$ Hz were obtained, which are shown in Fig. 10b. For the assessment of the potential convergence speed of the algorithm, an experiment was carried out for $\nu = 0.1$ Hz, $\underline{\rho} = 5\text{e-}5$ rad (5 mm), employing an increased gain of $k_q = 5\text{e-}7$ and a maximum control value of $\bar{v}_\text{c} = 3\text{e-}5$ rad/s. The related results are shown in Fig. 10c.

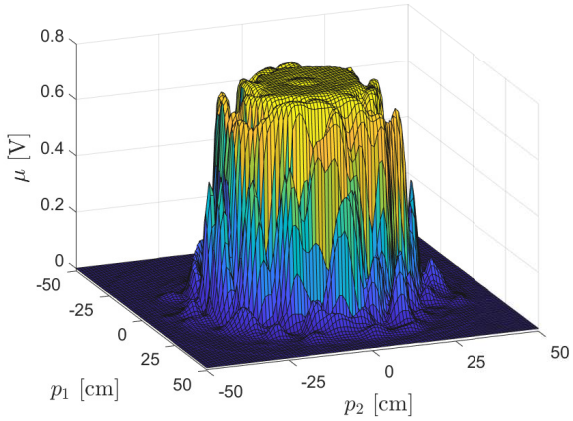


Figure 7. The distribution of the laser beam intensity in the vicinity of the detector obtained with spiral trajectory for $r = 3\text{e-}6$ rad/s, $\omega = 0.31$ rad/s and $d = 100$ m.

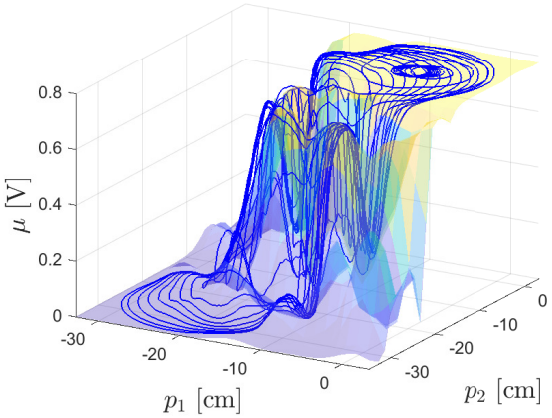


Figure 8. Paths in the configuration space during the phase of gradient-based control for $\nu = 0.1$ Hz, $k = 2\text{e-}7$, $\bar{v}_c = 1\text{e-}5$ rad/s, $\underline{\rho} = 2\text{e-}4$ rad.

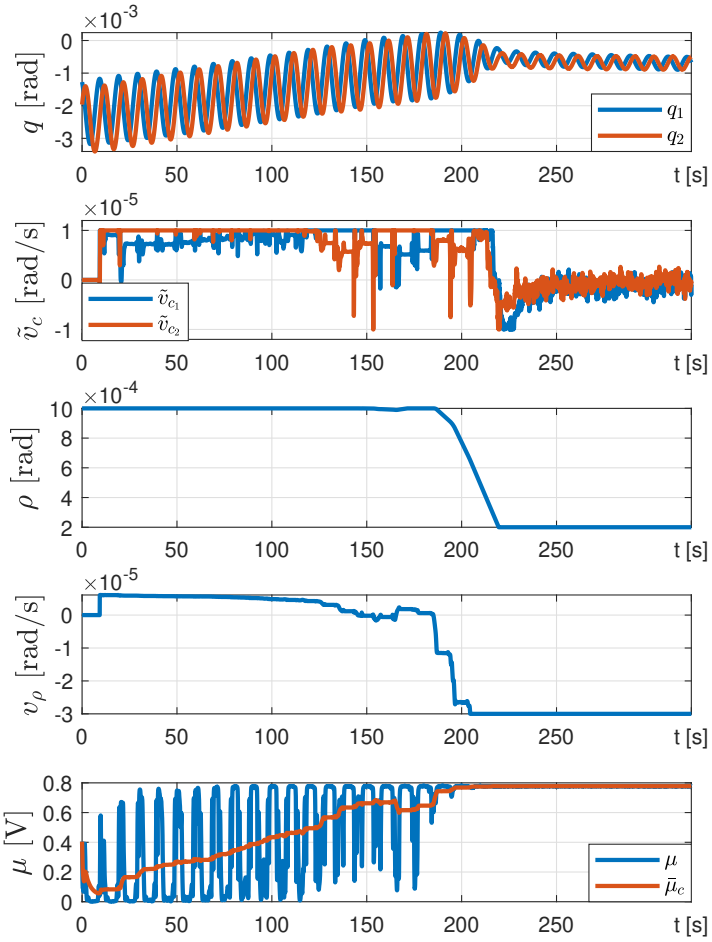


Figure 9. Time plots of configuration q, input $\tilde{v}_c$ and laser beam intensity μ during the phase of gradient-based control for $\nu = 0.1$ Hz, $k_q = 2\text{e-}7$, $\bar{v}_c = 1\text{e-}5$ rad/s, $\underline{\rho} = 2\text{e-}4$ rad.

5 Summary

In this paper, the extremum-seeking control algorithm, aimed at optimizing the orientation of a laser transmitter to maximize the signal-to-noise factor, assuming that measurements of the beam position are unavailable, is proposed. The algorithm takes advantage of the open-loop covering stage and the closed-loop method based on continuous approximations of the gradient in a two-dimensional configuration space. We formally show that the algorithm ensures the convergence of the system configuration to a set in which the intensity of the received signal is close to its maximum.

Through experimental research, we have successfully demonstrated that the method can be efficiently implemented and provides all the assumed characteristics across a wide range of parameter values. In particular, the conducted experiments confirm a high positioning precision achievable with the custom-made two-axis astronomical mount, that is dedicated to astronomical and satellite observations. The system has also been tested in a tracking mode, where the position of the receiver changes over time.

Our future work will focus on enhancing the method through recovery and identification of a model of the intensity function. Additionally, we will investigate the robustness of the method against measurement uncertainties and limited sampling frequency. We also plan to improve system performance in dynamic scenarios by reducing time delays, accelerating the acquisition of the intensity signal, and applying the method to a new fast opto-mechanical system specifically designed for this purpose.

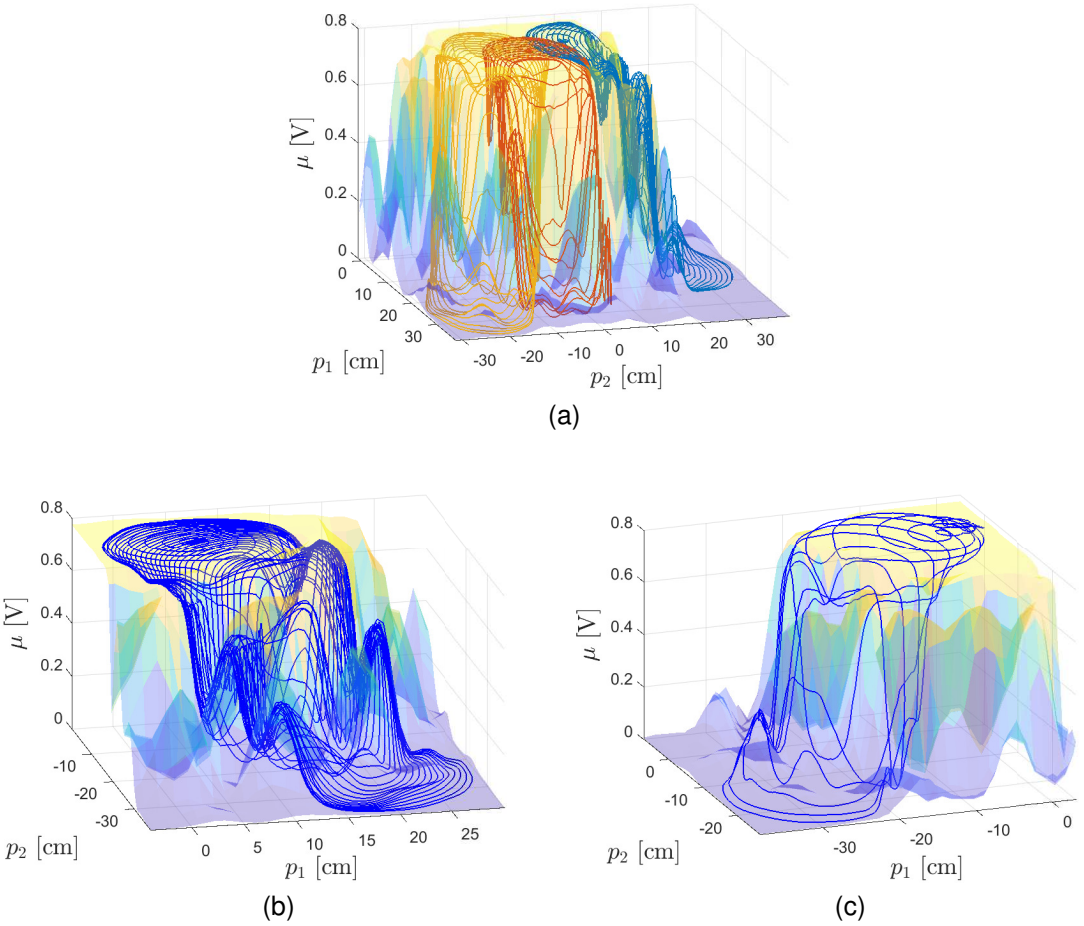


Figure 10. Path in the configuration space during the phase of gradient-based control for: (a) $\nu = 0.1$ Hz, $k = 2\text{e-}7$, $\bar{v}_c = 1\text{e-}5$ rad/s, $\underline{\rho} = 5\text{e-}5$ rad; (b) $\nu = 0.2$ Hz, $k_q = 2\text{e-}7$, $\bar{v}_c = 1\text{e-}5$ rad/s, $\underline{\rho} = 5\text{e-}5$ rad; (c) $\nu = 0.1$ Hz, $k_q = 5\text{e-}7$, $\bar{v}_c = 3\text{e-}5$ rad/s, $\underline{\rho} = 5\text{e-}5$ rad.

Data availability

The data used in this study are available upon request from the corresponding author via email.

References

1. Ye, J. *et al.* Research on quadrant detector multi-spot position detection based on orthogonal frequency division multiplexing. *Appl. Sci.* **13**, DOI: 10.3390/app132312826 (2023).
2. Zinchenko, S., Moiseienko, V., Tovstokoryi, O., Nosov, P. & Popovych, I. Automatic beam aiming of the laser optical reference system at the center of reflector to improve the accuracy and reliability of dynamic positioning. In Hu, Z., Petoukhov, S., Dychka, I. & He, M. (eds.) *Advances in Computer Science for Engineering and Education IV*, 3–14 (Springer International Publishing, Cham, 2021).
3. Zhou, W., Jin, K. & Zhang, R. A fast-speed gmppt method for pv array under gaussian laser beam condition in wireless power transfer application. *IEEE Transactions on Power Electron.* **37**, 10016–10028, DOI: 10.1109/TPEL.2022.3155726 (2022).
4. Watanabe, K., Koyama, T., Koga, H., Izumi, K. & Tsujimura, T. Robotic alignment technique of search control for laser beam communication. In *2022 61st Annual Conference of the Society of Instrument and Control Engineers (SICE)*, 258–263, DOI: 10.23919/SICE56594.2022.9905838 (2022).
5. Affan Ahmed, S., Mohsin, M. & Zubair Ali, S. M. Survey and technological analysis of laser and its defense applications. *Def. Technol.* **17**, 583–592, DOI: 10.1016/j.dt.2020.02.012 (2021).

6. Nikulin, V., Khandekar, R. & Sofka, J. Agile acousto-optic tracking system for free-space optical communications. *Opt. Eng.* **47**, 064301, DOI: 10.1117/1.2947581 (2008).
7. Laas-Bourez, M., Coward, D., Klotz, A. & Boër, M. A robotic telescope network for space debris identification and tracking. *Adv. Space Res.* **47**, 402–410, DOI: 10.1016/j.asr.2010.09.010 (2011).
8. Nikulin, V. V., Bouzoubaa, M., Skormin, V. A. & Busch, T. E. Modeling of an acousto-optic laser veam steering system intended for satellite communication. *Opt. Eng.* **40**, 2208 – 2214, DOI: 10.1117/1.1403022 (2001).
9. Kaushal, H. & Kaddoum, G. Applications of lasers for tactical military operations. *IEEE Access* **5**, 20736–20753, DOI: 10.1109/ACCESS.2017.2755678 (2017).
10. Frączek, E., Frączek, W. & Popiołek-Masajada, A. Laser beam positioning by using a broken-down optical vortex marker. *Appl. Sci.* **11**, DOI: 10.3390/app11167677 (2021).
11. Krstic, M. Performance improvement and limitations in extremum seeking control. *Syst. & Control. Lett.* **39**, 313–326, DOI: 10.1016/S0167-6911(99)00111-5 (2000).
12. Krstic, M. & Ariyur, K. *Real-Time Optimization by Extremum-Seeking Control* (John Wiley & Sons, Hoboken, New Jersey, 2003).
13. Danielson, C., Bortoff, S. A. & Chakrabarty, A. Extremum seeking control with an adaptive gain based on gradient estimation error. *IEEE Transactions on Syst. Man, Cybern. Syst.* **53**, 152–164, DOI: 10.1109/TSMC.2022.3171132 (2023).
14. Gelbert, G., Moeck, J. P., Paschereit, C. O. & King, R. Advanced algorithms for gradient estimation in one- and two-parameter extremum seeking controllers. *J. Process. Control.* **22**, 700–709, DOI: 10.1016/j.jprocont.2012.01.022 (2012).
15. Wepener, D., le Roux, J. D. & Craig, I. Extremum seeking control of a flotation circuit using peak air recovery. *IFAC-PapersOnLine* **55**, 61–66, DOI: 10.1016/j.ifacol.2022.09.244 (2022). 19th IFAC Symposium on Control, Optimization and Automation in Mining, Mineral and Metal Processing MMM 2022.
16. Benosman, M. Learning-based adaptive control for nonlinear systems. In *2014 European Control Conference (ECC)*, 920–925, DOI: 10.1109/ECC.2014.6862378 (2014).
17. Liu, S.-J. & Krstic, M. *Stochastic Averaging and Stochastic Extremum Seeking* (Springer London, 2012).
18. Tan, Y., Nesic, D., Mareels, I. & Astolfi, A. On global extremum seeking in the presence of local extrema. In *Proceedings of the 45th IEEE Conference on Decision and Control*, 5663–5668, DOI: 10.1109/CDC.2006.377791 (2006).
19. Santos, G. C. & Oliveira, T. R. Gradient extremum seeking with nonconstant delays. *IEEE Access* **8**, 120429–120446, DOI: 10.1109/ACCESS.2020.3005186 (2020).
20. Kozłowski, K. *et al.* High precision automated astronomical mount. In *Automation 2019*, 299–315 (Springer International Publishing, Cham, 2020).
21. Bartkowiak, P., Patelski, R., Kwiatkowska, M. & Pazderski, D. System architecture for development and supervision of robotic astronomical telescope. *Pomiary Autom. Robotyka* **26**, 43–51, DOI: 10.14313/PAR_246/43 (2022).
22. Patelski, R. & Pazderski, D. Tracking control for a cascade perturbed control system using the active disturbance rejection paradigm. *Arch. Control. Sci.* **29**, 387–408, DOI: 10.24425/acs.2019.129387 (2019).

Funding

This work was supported by Poznan University of Technology grant number 0211/SBAD/0125 and by the *PhDBoost* Program for doctoral students of the Doctoral School of Poznan University of Technology (in 2024) from the University's subsidy financed from the funds of Ministry of Science and Higher Education.

Author contributions statement

P.B. contributed to conceptualization, methodology, and formal analysis; hardware implementation and conducting the experiments; data analysis and visualization; and writing—original draft preparation, review, and editing. D.P. contributed to conceptualization, methodology, and formal analysis; hardware preparation; and writing—original draft preparation, review, and editing. All authors reviewed and approved the final version of the submitted manuscript.

Competing interests

The authors declare no competing interests.